

Anticorrosive efficiency of alkyd resin-based coatings containing Mg–Zn–Fe mixed oxide-based pigments

Antikoroziční účinnost nátěrových hmot na bázi modifikované alkydové pryskyřice s obsahem směsných oxidů Me–Zn–Fe

Kalendová A., Halecká E., Nechvilová K., Kohl M.

University of Pardubice, Faculty of Chemical Technology, Institute of Chemistry and Material Technology, Department of Painting and Organic Coatings

E-mail: andrea.kalendova@upce.cz

Mixed oxide-based pigments Mg–Zn–Fe with different particle morphologies were prepared by high-temperature solid phase reactions. The core shell pigments containing ferric oxide and non-isometric particles of layered silicates were also prepared. The pigments were tested in paints, the pigment volume concentrations in the modified alkyd resin based binder being 5%, 10%, and 15%. The paint properties were examined by accelerated corrosion tests and by physico-mechanical tests. The effect of the pigment particle morphology on the surface hardness of the paint films was also studied. The influence of pigment volume concentration on the coating properties, and the optimum concentrations providing the most efficient anticorrosive protection were processed. A higher anticorrosion efficiency was observed for the paints with pigments possessing the lamellar particle shape.

Byly syntetizovány směsné oxidy kovů Mg–Zn–Fe s různou morfologií částic reakcí v pevné fázi za vysokých teplot. Rovněž byly připraveny jádrové core-shell pigmenty s obsahem feritů na neizometrických částicích nosiče na bázi vrstevnatých křemičitanů. Vlastnosti feritů byly zjišťovány v pojivu nátěrové hmoty na bázi alkydové pryskyřice při objemových koncentracích 5%, 10 a 15%. Vlastnosti nátěrů byly testovány pomocí zrychlených korozních a fyzikálně mechanických testů. Byl hodnocen rovněž vliv morfologie částic na povrchovou tvrdost nátěrů. Byl sledován vliv objemové koncentrace pigmentů na vlastnosti nátěrů a byla zjišťována optimální koncentrace pigmentů zajišťující maximální protikoroziční ochranu. Nejvyšší antikoroziční účinnost byla vyhodnocena v případě nátěrů s obsahem pigmentů vykazující lamelární tvar částic.

INTRODUCTION

Metals are routinely protected against atmospheric corrosion by coating their surface with a liquid organic paint, which forms a firm, consistent and well-adhering polymeric film by curing polymerisation reactions [1]. As experimental knowledge implies, the mere barrier protection of both non-pigmented and pigmented coatings with barrier pigments does not suffice to achieve the high protective efficiency required of metal anticorrosion protection in an aggressive environment [2]. The efficient solution of anticorrosion metal protection is offered by the formation of complex protecting coating systems consisting of a base paint with the content of nontoxic anticorrosion pigments of inorganic nature and of a top coat that ensures pronounced barrier effects and contains substances preventing the decomposition of a binder

exposed to UV radiation [3,4]. The protective properties of organic coatings are dependent, among other factors, on their impermeability to liquids and gases [5-7]. Protective film impermeability to liquids and gases can be improved by using nonisometric fillers [8,9]. Among pigments exhibiting nonisometric particle morphology are also some core-shell pigments [10,11].

The anticorrosion pigments that used to be applied in the past, however, were not very environmentally friendly, and efforts are nowadays made to develop and manufacture pigments that are free from toxic heavy metals such as Pb, Cd, Ba and Cr(VI) [2,12,13]. Among rather new inorganic anticorrosive pigments are ferrosin type pigments, finding application as pigments to protect the metal materials against corrosion [14]. An efficient anticorrosive pigment will not only possess good corrosion-inhibition properties but it will

also have a favourable effect on the paint film's mechanical resistance [15,16]. The particle shape and size of, e.g., spinel type compounds depend on the method of synthesis and on the conditions of the process [17,18]. The following factors play a major role in the conventional calcination methods—of ferrites: particle size, crystal modification, morphology, and specific surface area [19-22]. The resulting ferros spinels were found to retain particle morphology of the initial iron oxides [23]. The most efficient anticorrosive ferrites include ferros spinels containing zinc and magnesium in specific ratio. It has been found that ferrites with Mg^{2+} and Zn^{2+} as the divalent cations exhibit a very good anticorrosive efficiency, especially if their molar ratio is 0.2:0.8 [24,25].

The aim of this study was to synthesize and investigate the properties of Mg–Zn–Fe ferros spinel based pigment possessing different particle morphologies with the goal to prepare such paints pigmented with them as exhibit a high mechanical and corrosion inhibition properties. Core-shell pigments containing silicate cores and Mg–Zn–Fe shell were also synthesized and studied with focus on their properties in organic protective coatings in a simulated corrosive environment. The particle morphology of such pigments is dictated by the core particle shape and size, affecting the physical properties and barrier properties of the organic coating in corrosive environments [11, 25, 26]. Layered silicates, specifically talc and calcined kaolin, exhibited differences in the composition, physical properties of their surface, and particle texture, which may affect the pigment properties in the paints [27, 28].

EXPERIMENTAL

Pigment synthesis

The pigments were formulated as the oxides $Mg_{0.2}Zn_{0.8}Fe_2O_4$ possessing a spinel structure. Many ferrite type pigments possessed variable combinations of the divalent cations Zn and at different molar ratios in the elementary spinel lattice [29]. Efforts were made during the synthesis of the ferros spinel $Mg_{0.2}Zn_{0.8}Fe_2O_4$ ("Pig A") to achieve the spinel structure and isometric particles. Therefore, $\alpha-Fe_2O_3$ (hematite; density 5.1 g cm^{-3} ; colour red; relative molecular weight M_r $159.69 \text{ g mol}^{-1}$; mean particle size $0.546 \text{ }\mu\text{m}$), whose particles are regularly nodular, was used as the starting material. The aim of the synthesis of the next ferros spinel $Mg_{0.2}Zn_{0.8}Fe_2O_4$ ("Pig B") was to obtain a with a nonisometric – specifically needle-shaped – particle morphology. Goethite ($\alpha-FeO(OH)$; density 4.1 g cm^{-3} ; colour yellow; M_r $88.85174 \text{ g mol}^{-1}$; mean particle size $0.901 \text{ }\mu\text{m}$), with needle-shaped particles, was used as the ferric oxide source. The third $Mg_{0.2}Zn_{0.8}Fe_2O_4$ ("Pig C") was prepared by an identical procedure with the aim to prepare

a nonisometric spinel pigment with a lamellar particle shape. Specularite, a ferric oxide with a lamellar particle structure (hematite structure; Fe_2O_3 content 98%; 2% clinocllore; colour silver grey; mean-particle size $53.57 \text{ }\mu\text{m}$), was used as the starting material.

Solid state reaction by calcination of the starting substances at high temperatures was chosen for the synthesis. The synthesis procedure consisted of a number of steps, including homogenisation of the starting mixture, calcination, rinsing, milling, and drying [12]. The calcination was conducted as a two-stage procedure: the pigments were first calcined at 1000°C for 2 hours and then at 1180°C . In order to obtain the right pigment particle size for use in paints, the calcinate was subjected to wet milling in a planetary ball mill (Pulverisette 6, Netzsch, Germany).

The core shell type pigments ("Pig D" and "Pig E") were synthesized by applying the matrix core (kaolin, talc) to mixed oxide (Mg–Zn–Fe, shell) weight ratio 1:1. The core shell type pigments (the mixed Mg–Zn–Fe oxides forming the functional layer on the core) were also synthesized by high temperature solid-phase reaction, by two-stage calcination like the non core ferros spinels [30,31]. Kaolin (calcined kaolin; the majority fraction consisted of amorphous metakaolin, the minority phase consisted of crystalline α -quartz SiO_2 , cristobalite and mullite $Al_6Si_2O_{13}$; white colour; density 2.71 g cm^{-3} ; manufactured by CLUZ a.s. Czech Republic; mean particle size $10.30 \text{ }\mu\text{m}$) and talc (pure talc $Mg_3(OH)_2(Si_4O_{10})$; density 2.71 g cm^{-3} ; mean particle size $13.71 \text{ }\mu\text{m}$), i.e. materials exhibiting a lamellar particle shape, were used as the mineral carriers (cores).

Determination of the physico-chemical properties of the powdered pigments

Structural purity of the products was checked and their X-ray diffraction spectra were measured on a D8 Advance Diffractometer (Bruker AXS). The pigment particle surface and shape were examined on a JEOL-JSM 5600 LV scanning electron microscope (JEOL, Japan). A helium AutoPycnometer 1320 (Micromeritics, USA) was used to determine the pigments' specific weight (ρ_p). Linseed oil consumption (on_p) was measured by the pestle-mortar method. The result of the measurement, the oil number (in $\text{g}\cdot 100\text{g}^{-1}$), is a necessary quantity for calculation of the CPVC and for the formulation of coating materials [29]. The pH of aqueous extracts of the pigments (pH_p) was measured in accordance with ISO 789-9 by preparing 10 wt.% pigment suspensions in redistilled water ($\text{pH} = 6.5$). Specific electric conductivity of aqueous extracts of the pigments (χ_p) was measured conductometrically in 10% suspensions of the pigments in redistilled water (specific electric conductivity = $3 \text{ }\mu\text{S cm}^{-1}$) in conjunction with calibration solutions (conductivity 37 and $1413 \text{ }\mu\text{S cm}^{-1}$ at 25°C).

This procedure was based on the ISO 787-14 standard [32,33]. A Mastersizer 2000 particle size analyser was used for determination of the particle size distribution.

Determination the anticorrosion efficiency of the pigments in paints

In order to assess their potential anticorrosion efficiency, the pigments were added to a solution of an alkyd resin modified with soy oil (density 1.1 g cm^{-3} , dry matter fraction 58.9%). The pigment volume concentrations (PVC) selected for the paints were 5%, 10% and 15%. The PVC/CPVC ratio (CPVC = critical PVC) was invariably adjusted to 0.35 by using limestone (CaCO_3) as an anticorrosive-neutral filler. Cobalt octoate at a fraction of 0.3 wt.% was used as the siccative. The paints were prepared by dispersing the pigment, using the pearl mill Dispermat CV (WMA Getzmann GmbH, Verfahrenstechnik, Germany) filled with glass pearls of 2-mm diameter as the grinding medium.

Test samples were prepared by coating test steel panels (deep-drawn cold-rolled steel manufactured by Q-panel, UK) $150 \text{ mm} \times 100 \text{ mm} \times 0.9 \text{ mm}$ size with the paints by means of a box-type application ruler $200 \mu\text{m}$ slot width as per ISO 1514. The dry film thickness (DFT) was measured with a magnetic thickness gauge (Elektrophysik, Germany) as per ISO 2808. Ten panels were prepared for each paint.

A thin line (7 cm long and 0.5 mm width) and penetrating as deep as the substrate was cut into the paint film by using a sharp blade [34]. The paint films on the panels were allowed to dry in standard conditions ($21^\circ\text{C} \pm 2^\circ\text{C}$, 50% relative humidity RH) for 6 weeks in an air-conditioned laboratory.

Laboratory corrosion tests

The cyclic corrosion test in an atmosphere with condensing water was performed as per CSN EN ISO 6270. In this test the test panels were exposed to condensed water at 40°C for 12 hours and dried at 23°C also for 12 hours [35]. The samples were evaluated after 1008 hours' exposure. The cyclic corrosion test in an environment with a NaCl mist was based on ISO 7253. In this test the test panels were exposed to the mist of a neutral 5% NaCl solution at 36°C for 10 hours (1st cycle stage) and to condensing water at 40°C for 1 hour (2nd cycle stage), followed by drying at 23°C for 1 hour (3rd cycle stage) [36].-

After the corrosion tests the paints were evaluated by methods derived from ASTM D 714-87, ASTM D 610 and ASTM D 1654-92 standards [36]. The following corrosion phenomena were assessed: formation of blisters on the film (their size and number); extent of corrosion across in the substrate metal surface observed after removing the film (percent area fraction affected);

extent of propagation (in mm) of corrosion of the substrate metal near a cut made in the film, observed after removing the film; and formation of blisters on the film near the cut made in it (their size and number). The test results were translated into scores on a 100-point scale and combined together to obtain what we refer to as the overall anticorrosion efficiency of the pigmented coating. The overall anticorrosion efficiency for all the tests performed ($E_{\text{H}_2\text{O}}$, E_{NaCl}) was calculated in the same manner as the arithmetic mean from the corrosion effects observed [37].

Effect of the pigments on the physico-mechanical properties of the organic coatings

Resistance of the paint film against cupping was made in an Erichsen cupping tester (ISO 1520). The cupping (in mm) giving rise to the first signs of disturbance of the paint film was measured [38,39]. The physico-mechanical evaluation was carried out after application on steel panels – size $152 \times 75 \times 0.8 \text{ mm}$ (Standard low-carbon steel panels S-36, Q-Lab Corporation).

Determination of the effects of pigmented particles on the surface hardness of paints

Determination of the surface hardness of the paint film on glass panels ($100 \times 200 \times 5 \text{ mm}$) was performed on Perzos-type pendulum device. The unit of measure of hardness is given in percents related to the hardness of a glass standard whose hardness represents 100 % [40]. The first measurements were made 24 hours after paint application to the glass panels and continued till day 40, after which no significant surface hardness changes took place any more [41].

RESULTS AND DISCUSSION

Pigment structure and morphology

Morphology of the pigment particles synthesised is shown in the SEM photographs in Fig. 1. The results of the X-ray diffraction analysis of the pigments synthesised are given in Tab. 1. The aim of the synthesis of the pigments *Pig A*, *Pig B* and *Pig C* was to obtain pigments possessing the spinel structure whose chemical formula is $\text{Mg}_{0.2}\text{Zn}_{0.8}\text{Fe}_2\text{O}_4$. These three pigments are also referred to as *Pig A* (isometric $\text{Mg}_{0.2}\text{Zn}_{0.8}\text{Fe}_2\text{O}_4$), *Pig B* (acicular $\text{Mg}_{0.2}\text{Zn}_{0.8}\text{Fe}_2\text{O}_4$), and *Pig C* (lamellar $\text{Mg}_{0.2}\text{Zn}_{0.8}\text{Fe}_2\text{O}_4$), respectively, throughout this text. Mixed spinel ferrites containing zinc and magnesium cations constituted the majority phases. The magnesium atoms can be isomorphically substituted by zinc atoms, owing to which the mixed spinels can be formed across an unlimited range of concentrations. The magnesium-to-

zinc cation ratio could not be determined precisely from the analysis because the lattice parameters in $MgFe_2O_4$ and $ZnFe_2O_4$ approach each other and the diffraction lines may overlap. The X-ray analysis of the pigments *Pig A*, *Pig B* and *Pig C* did not exhibit any crystal phases of the starting materials, in other words, the starting materials had completely reacted to the products [42]. Furthermore, the 3 spinel types were synthesized with a view to obtaining pigments $Mg_{0,2}Zn_{0,8}Fe_2O_4$ possessing different particle shapes, making use of the different particle shapes of the starting ferric oxide types: the particles of pigment *Pig A* ($Mg_{0,2}Zn_{0,8}Fe_2O_4$), were *isometric*, the particles of pigment *Pig B* ($Mg_{0,2}Zn_{0,8}Fe_2O_4$) were needle-shaped (*acicular*), and the particles of pigment *Pig C* ($Mg_{0,2}Zn_{0,8}Fe_2O_4$) were *lamellar*.

The core-shell pigment *Pig D* ($Mg_{0,2}Zn_{0,8}Fe_2O_4$ /kaolin or $Mg_{0,2}Zn_{0,8}Fe_2O_4/Al_6Si_2O_{13}$) was prepared as a pigment whose nonisometric (*lamellar*) core particles of calcined kaolin are dispersed with a functional shell of the mixed oxide $Mg_{0,2}Zn_{0,8}Fe_2O_4$. For this, the starting materials for the shell were mixed in proportions providing the Mg–Zn–Fe cation ratio 0.2:0.8:2. Mixed oxides of aluminium, iron and magnesium were identified (*hercynite*). The analysis gave evidence that chemical reactions had occurred between the kaolin surface and the remaining starting materials: indeed, the mixed oxide *hercynite* ($FeMg_3Al_2O_4$) contains the alu-

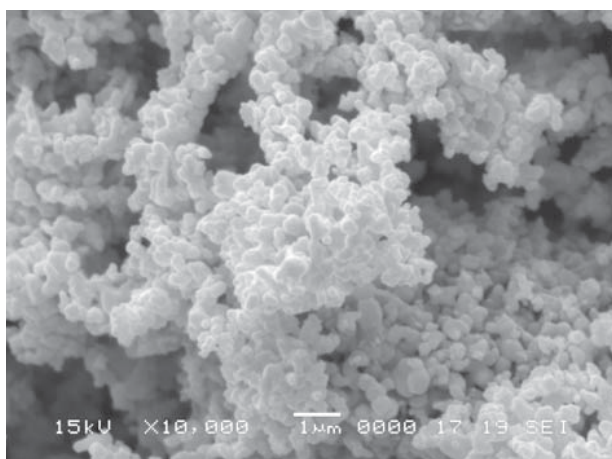
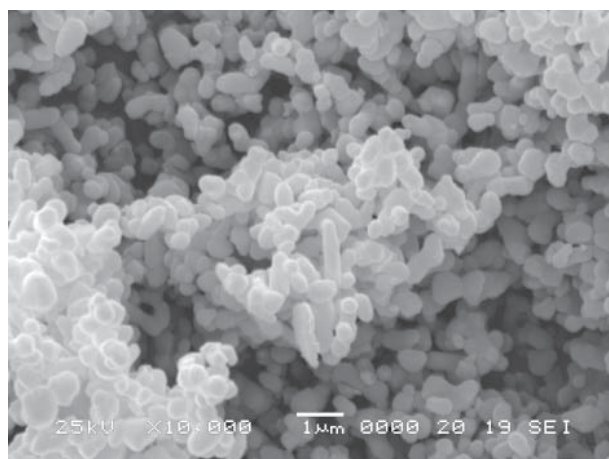
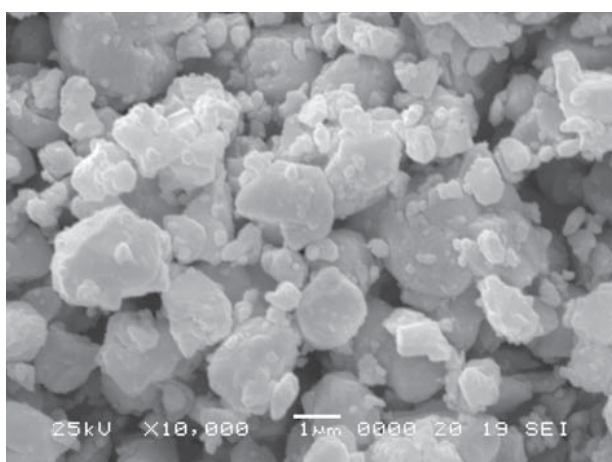
minium cation, which initially was present in the starting kaolin. The X-ray diffraction analysis showed that the pigment also included silicates ($MgSiO_3$) and crystalline silicon oxide (SiO_2) phases (*crystalite*) from the starting kaolin. The resulting pigment *Pig D* exhibited a *lamellar* particle shape (Fig. 1). Pigment *Pig E* ($Mg_{0,2}Zn_{0,8}Fe_2O_4$ /talc or $Mg_{0,2}Zn_{0,8}Fe_2O_4/Mg_3(Si_4O_{10})(OH)_2$) was synthesized with a view to obtaining a core-shell pigment where the mixed Mg–Zn–Fe oxide shell covers a mineral core possessing a *lamellar* particle structure, specifically talc ($Mg_3(OH)_2Si_4O_{10}$). The highest diffraction line belonged to the crystalline ferrite phase. As in the remaining pigments, isomorphic replacement of the zinc cation by a magnesium cation had occurred in this ferrite layer, and so their precise ratio could not be determined. Components of minor importance in this pigment included magnetite (Fe_3O_4) from the starting hematite, and the silicon dioxide *crystalite* from talc in the core. The synthesized pigments *Pig D* and *Pig E* were referred in this work as the core shell type pigments [30,31,33].

Comparison experiments

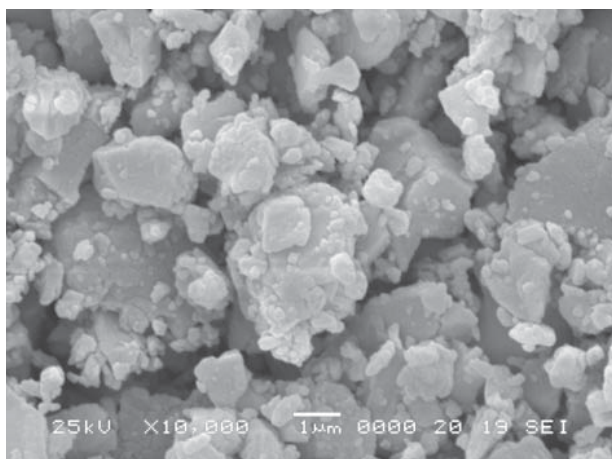
The starting hematite was also examined (*Pig F*). The non-pigmented organic coating material was subjected to the mechanical resistance tests and corrosion tests as well.

Tab. 1. Results of X-ray diffraction analysis of the pigments / Výsledky rentgenové difrakční analýzy

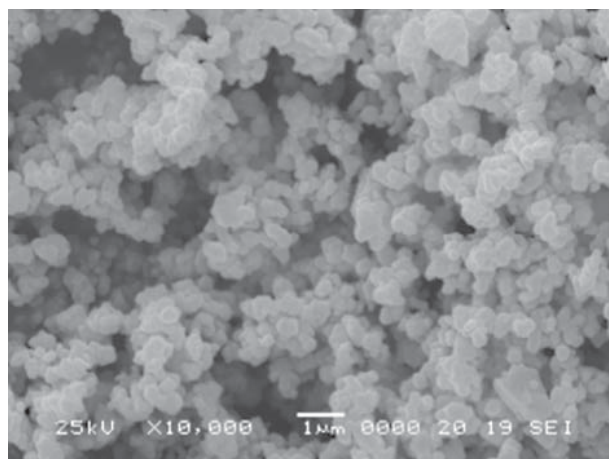
Pigment type	Identified the crystal phase of the pigment		Crystal structure	The lattice parameters		
				a	b	c
Pig A $Mg_{0,2}Zn_{0,8}Fe_2O_4$ isometric	$Zn_{0,98}Fe_{1,99}O_4$	Franklinite	cubic	8.43800	8.43800	8.43800
	$Mg_{0,4}Zn_{0,6}Fe_2O_4$	–	cubic	8.42700	8.42700	8.42700
	$Zn_{0,94}Fe_{1,99}O_4$	–	cubic	8.43300	8.43300	8.43300
Pig B $Mg_{0,2}Zn_{0,8}Fe_2O_4$ acicular	$Zn_{0,98}Fe_{1,99}O_4$	Franklinite	cubic	8.43800	8.43800	8.43800
	$Mg_{0,4}Zn_{0,6}Fe_2O_4$	–	cubic	8.42700	8.42700	8.42700
	$Zn_{0,94}Fe_{1,99}O_4$	–	cubic	8.43300	8.43300	8.43300
Pig C $Mg_{0,2}Zn_{0,8}Fe_2O_4$ lamellar	$Zn_{0,98}Fe_{1,99}O_4$	Franklinite	cubic	8.43800	8.43800	8.43800
	$Mg_{0,4}Zn_{0,6}Fe_2O_4$	–	cubic	8.42700	8.42700	8.42700
	$Zn_{0,94}Fe_{1,99}O_4$	–	cubic	8.43300	8.43300	8.43300
Pig D Mg–Zn–Fe mixed oxide//kaolin	$Fe_{1,84}Al_{0,16}O_3$	–	rhombic	8.13960	8.13960	8.13960
	$Fe_{0,76}Mg_3Al_{1,94}O_4$	Hercynite	kubická	4.99340	4.99340	7.00550
	SiO_2	Cristobalite	tetragonal	4.91458	4.91458	5.40649
	SiO_2	Quartz	hexagonal	4.15600	4.15600	2.66010
	SiO_2	Stisovite	tetragonal	8.13960	8.13960	8.13960
Pig E Mg–Zn–Fe mixed oxid//talc	$MgFe_2O_4$	Magnesianoferrite	cubic	8,39500	8,39500	8.39500
	Fe_3O_4	Magnetite	cubic	8,39600	8,39600	8.39600
	SiO_2	Cristobalite	tetragonal	4.99340	4.99340	7,00550
	$MgSiO_3$	Enstatite	orthorhombic	8.23000	8.84000	5.19000
	$CaMgSi_2O_6$	Diopside	monoclinic	9.51970	8.70960	5.14960

a) $Mg_{0.2}Zn_{0.8}Fe_2O_4$ isometricb) $Mg_{0.2}Zn_{0.8}Fe_2O_4$ acicularc) $Mg_{0.2}Zn_{0.8}Fe_2O_4$ lamellar

d) Mixed oxide Mg-Zn-Fe/kaoline



e) Mixed oxide Mg-Zn-Fe/talc



f) Hematite

Fig. 1. Morphology of the particles of tested pigments (SEM)
 Obr. 1. Morfológie částic testovaných pigmentů (SEM)

Description of the pigments with respect to their physico-chemical properties

Table 2 includes the following pigment parameters: density (ρ_p), oil number (on_p), CPVC, pH (pH_p), and

specific electric conductivity (χ_p) of aqueous extracts of the powdered pigments. The core-shell pigment and ferrosin pigment densities lie within the ranges of $4.99\text{--}5.12\text{ g cm}^{-3}$ and $3.57\text{--}3.96\text{ g cm}^{-3}$, respectively. The particle size distribution values $D(0.5)$, $D(0.9)$,

and D(0.1) show that the size of 50%, 90% or 10% particles, respectively, in the volume is smaller than the specified value. Milling was a successful way to reduce the pigment particles to a size that is suitable for use as pigments in paints forming homogeneous films free from aggregations (Fig. 1).

Values of the oil consumption of the core-shell pigments lay within the range from 26 g 100 g⁻¹ pigment to 29 g 100 g⁻¹ pigment, as against the ferrosinels, where the levels ranged from 10.8 g 100 g⁻¹ pigment to 12.8 g 100 g⁻¹ pigment. The critical pigment volume concentration levels were calculated to be about 47 for the core-shell pigments and from 59% to 63% for the ferrites. CPVC is generally the maximum amount of the pigment with which the binder (here: linseed oil) is still capable of forming a consistent and coherent film. The lamellar core-shell pigments exhibited lower CPVCs than their "non-core-shell" counterparts [43,44].

The efficiency of an anticorrosive pigment is pH dependent [45,46]. The pH of a pigment dispersed in a paint film should not exceed the alkalinity level at which the ester bonds in the alkyd resin paint binder may undergo chemical degradation. A higher alkalinity – pH 10.0 – was found for pigment *Pig C* (lamellar Mg_{0.2}Zn_{0.8}Fe₂O₄). This is presumably due to the presence of a residual amount of the unreacted magnesite (below the limit of detection by the X-ray method) because magnesium carbonate is very difficult to decompose [47]. Such pigments, possessing a high pH, can be expected to form alkaline soaps with the acid components of the alkyd resin (a fatty acid R-COOH in this case) and to enter other neutralization reactions with the acid components of the

corrosive medium penetrating through the protective film. A higher alkalinity (pH 9.1) was also measured for the core-shell pigment *Pig E* (mixed Mg–Zn–Fe oxide/talc), and so an active chemical action in the paint film was expected here also. The alkalinity of this pigment is affected by the ferrite layer deposited on the core. This is beneficial with respect to the pigment's anticorrosive effect, because alkalinity at the film–metallic substrate interface does not support corrosion (i.e. corrosion proceeds faster in an acid environment [48,49]). A slightly acid pH (pH 5.9), was measured in the aqueous extract of the reference pigment *Pig F* (hematite Fe₂O₃), which (unlike the ferrites) does not contain cations of alkaline nature. This industrial pigment also exhibited a very low conductivity of the aqueous extract (52 μS cm⁻¹).

The specific electric conductivity values (χ_p) of the ferrosinels and of the core-shell pigments lay within the ranges of 71–114 μS cm⁻¹ and 104–132 μS cm⁻¹, respectively. The alkaline nature of the pigments *Pig C* (lamellar Mg_{0.2}Zn_{0.8}Fe₂O₄) and *Pig E* (Mg–Zn–Fe oxide/talc) also induced the highest specific electric conductivity levels within their ranges, i.e. 114 and 132 μS cm⁻¹, respectively. Overall, the pigments exhibited low specific electric conductivity (Tab. 2).

Mechanical resistance tests of the paint films containing the pigments

Outstanding mechanical properties constitute a precondition for good anticorrosion efficiency of a paint film. Table 3 presents the results of the cupping test of the paints films containing the pigments. The objective

Tab. 2. Physico-chemical properties of the powdered pigments (density ρ_p , oil number on_p , CPVC, pH_p , specific electric conductivity χ_p) / Fyzikálně - chemické vlastnosti testovaných pigmentů v práškovém stavu (hustota, olejové číslo, KOKP, pH, měrná elektrická vodivost)

Pigment	Particle size per cent fraction below the specified size (μm)			^a ρ_p (g cm ⁻³)	^a on_p (g 100 g ⁻¹)	CPVC (%)	^a pH _p (-)	^b χ_p (μS cm ⁻¹)
	D(0.5)	D(0.9)	D(0.1)					
Pig A Mg _{0.2} Zn _{0.8} Fe ₂ O ₄	0.489	1.597	4.057	4.99	10.87	63.17	8.5	78
Pig B Mg _{0.2} Zn _{0.8} Fe ₂ O ₄	1.457	3.206	1.701	5.12	12.86	58.54	8.6	71
Pig C Mg _{0.2} Zn _{0.8} Fe ₂ O ₄	0.550	1.978	5.363	5.04	11.86	60.86	10.0	114
Pig D Mg–Zn–Fe mixed oxide/kaolin	1.300	3.200	4.100	3.57	29.30	47.05	7.8	104
Pig E Mg–Zn–Fe mixed oxide/talc	1.900	4.300	6.300	3.96	26.91	46.63	9.1	132
Pig F hematite Fe ₂ O ₃	0.399	1.623	5.123	5.05	19.84	48.15	5.9	52

^a Parameters are given as arithmetic averages within 10 measured values.

^a pH was measured with an accuracy ± 0.01, ^b Conductivity was measured with an accuracy ± 0.5%

of this test was to identify the resistance of the paint film against on-going deformation of a coated steel panel caused by indentation by a 20 mm steel ball. The films gave very good results in the cupping test, no film disturbance was observed with a magnifying glass after the body penetration to a 8 mm distance. The paint film resistance in this test was PVC-dependent, viz. so that the resistance against penetration decreased slightly with increasing PVC. Table 3 also demonstrates that the highest resistance against the test body penetration was obtained with pigment B (acicular $Mg_{0.2}Zn_{0.8}Fe_2O_4$), having needle-shaped particles viz. 9.5 mm at PVC = 5%. Good results were also obtained with the core-shell pigment E (mixed Mg–Zn–Fe oxide/talc), where the film was disturbed at 9.4 mm. The results give evidence that owing to their morphological properties, the pigments tested do not detract from the mechanical resistance of the alkyd resin based paints.

Results of the pigmented paint film surface hardness tests

The surface hardness data of the paint films on glass, measured by the pendulum method after Perzos, are listed in Table 3 (Parameters are given as arithmetic averages within 5 measured values). The paint film containing Pig A (isometric $Mg_{0.2}Zn_{0.8}Fe_2O_4$) exhibited

a higher surface hardness than the nonpigmented paint film throughout the entire test period and at any pigment volume concentration (PVC) – most at PVC = 10% (surface hardness 29.6% on Day 40). The higher surface hardness as compared both to the nonpigmented alkyd film and to the paint with Pig F (starting hematite) is an indirect indication of the presence of soaps formed by reaction between the unsaturated fatty acids and the zinc and magnesium cations [42].

The paint films containing Pig B (acicular $Mg_{0.2}Zn_{0.8}Fe_2O_4$) were slightly harder than the nonpigmented paint film. The paint film with PVC = 5% exhibited higher hardness than the nonpigmented film especially during the first phases of the drying process: in 2 days of drying, hardness of the paint with PVC = 5% and PVC = 10% was 9.5% and 9.2%, respectively. The higher Pig B (acicular $Mg_{0.2}Zn_{0.8}Fe_2O_4$) content of the paint slowed down the drying process slightly at the beginning. The highest surface hardness on Day 40 was observed for PVC = 10% (surface hardness 27.6%). A higher concentration (PVC = 15%) observably slowed the drying process down compared to the pigmented films with lower PVCs. This was due to the fact that oxygen penetrated more slowly through the film of this paint drying by the oxypolymerization mechanism. At the end of the measuring period, i.e. on Day 40, the paint films

Tab. 3. Paint film surface hardness test (DFT = 50 ± 10 μm), and results of mechanical tests of the paints (DFT = 60 ± 10 μm) / Povrchová tvrdost nátěrových filmů (DFT = 50 ± 10 μm) a fyzikálně – mechanické vlastnosti nátěrových filmů (DFT = 60 ± 10 μm)

Pigment	PVC (%)	Relative surface hardness of paints (%)							Cupping test (mm)
		(1. d)	(2. d)	(3.d)	(5. d)	(8. d)	(10. d)	(40. d)	
Pig A $Mg_{0.2}Zn_{0.8}Fe_2O_4$ isometric	5	7.4	8.8	11.1	15.6	22.0	21.0	28.7	8.9
	10	8.3	10.4	12.6	17.1	23.8	23.0	29.6	8.8
	15	8.0	10.4	11.9	14.6	22.8	22.8	29.5	8.8
Pig B $Mg_{0.2}Zn_{0.8}Fe_2O_4$ acicular	5	7.6	9.5	11.1	14.0	21.6	21.0	26.5	9.5
	10	7.2	9.2	11.1	13.1	20.3	21.1	27.6	9.2
	15	6.7	8.1	9.9	11.8	15.5	21.1	26.4	8.8
Pig C $Mg_{0.2}Zn_{0.8}Fe_2O_4$ lamellar	5	7.3	9.3	11.1	13.5	20.8	21.4	27.1	9.1
	10	6.6	8.4	9.6	11.8	14.5	16.7	27.3	8.8
	15	6.9	8.5	10.1	12.8	14.9	17.3	27.0	8.5
Pig D Mg–Zn–Fe mixed oxide/kaolin	5	7.1	9.1	10.7	13.6	18.4	20.3	26.2	9.3
	10	7.1	8.8	10.5	16.5	16.7	20.0	27.3	9.2
	15	7.2	8.7	10.3	13.4	16.0	18.0	26.0	8.8
Pig E Mg–Zn–Fe mixed oxide/talc	5	6.9	8.8	10.4	13.8	18.3	20.1	26.2	9.5
	10	7.1	8.8	10.0	14.1	17.4	19.9	26.0	9.0
	15	8.1	10.2	12.1	16.2	22.0	23.3	26.1	8.8
Pig F hematite Fe_2O_3	5	6.9	8.4	9.7	12.8	15.9	18.6	23.1	9.2
	10	8.0	9.5	11.1	16.7	20.9	21.6	25.5	9.2
	15	8.0	9.6	11.4	14.8	20.3	21.9	26.8	8.8
Non pig. paint	–	6.6	7.9	8.7	13.4	16.2	19.1	25.6	9.4

with *Pig C* (lamellar $Mg_{0.2}Zn_{0.8}Fe_2O_4$) exhibited a higher surface hardness than the nonpigmented film (about 27%). In the starting phases of the curing process, the film was cured somewhat slower if the paint contained the pigment in a higher concentration. On drying day 2, the hardness of the paint with PVC = 10% was 8.4% whereas at PVC = 5%, hardness was 9.3%. This was due to the lower rate of oxygen diffusion through the pigmented paint and hence, lower rate of alkyd resin drying by the oxypolymerization mechanism [50]. The highest hardness throughout the whole period was achieved with the paint film with PVC = 10% (27.3% on Day 40). The effect of the pigment, supporting the curing process and accelerating the drying process, was apparent at PVC = 10%. At PVC = 15%, however, the film curing process slowed down due to the reduced oxygen access, and so the surface hardness of that paint film was lower on Day 40 than the surface hardness of the paint films with lower PVCs (surface hardness 27%).

The presence of the core-shell *Pig D* in the binder brought about slight surface hardness increase against that of the nonpigmented paint. Surface hardness was highest at PVC = 10%, viz. 27.3%, which is more than the 26.0% surface hardness observed on the film with PVC = 15%. Hence, the optimum pigment volume concentration to improve the film's surface hardness is 10% (the paint film hardness attained in this case was 27.2%).

As to the paint films pigmented with the core-shell *Pig E* (mixed Mg–Zn–Fe oxide/talc), the relative surface hardness did not change appreciably with increasing PVC. Once the PVC = 10% was attained (surface hardness 26%), this paint's surface was harder than that of the nonpigmented film (25.6%). The surface hardness increase was supported by the ferrite layer on the otherwise soft talc-based core.

The paint film with the reference pigment *Pig F* (hematite Fe_2O_3) at PVC = 5% was "softer" than the nonpigmented binder throughout nearly the entire measuring period (23%). At PVC=5%, the binder itself played a more pronounced role in surface hardness than the pigment particles. This paint's surface hardness was mere 23.1% on Day 40. The role of the pigment particles was more marked at PVC = 15% (hardness 26.8%). Nevertheless, the hardness increase for the paint films with this reference pigment *Pig F* is not as marked as for the paint films with the pigments synthesized.

A more pronounced hardness increase was observed for the pigmented paint containing ferrite *A* (isometric $Mg_{0.2}Zn_{0.8}Fe_2O_4$). Surface hardness of the paint films at the end of the measuring period was 29.6 at PVC =10% and very similar, 29.5%, at PVC=15%.

The paint film with the reference pigment *Pig F* (hematite Fe_2O_3) at PVC =10% exhibited surface hardness of 25.5% only. In fact, this pigment did not contain any zinc (Zn^{2+}) or magnesium (Mg^{2+}) cations

capable of forming soaps and hence, could not affect the film hardness increase [51].

Owing to the regular shape of its particles, ferrite *Pig A* (isometric $Mg_{0.2}Zn_{0.8}Fe_2O_4$) was dispersed uniformly throughout the paint film. The diffusion rate of oxygen, which is essential in the paint drying (curing) process by the oxypolymerization mechanism, was not slowed down, and surface hardness of the film was higher than that of the paints containing the lamellar or needle-shaped ferrite pigments. This gives indirect evidence of the barrier effect against oxygen exhibited by the nonisometric ferrite types (pigments *B*, *C*).

It can be concluded that the isometric particles of the ferrites at PVC=15% facilitated the film curing process and contributed to the film hardness (at the time of measurement). The paint film surface hardness was 10.4%, 10.4%, and 8.8% at PVC=15%, PVC=10%, and PVC=5%, respectively, on the 2nd day of measurement.

The lamellar particles of the ferrites present at a high PVC (15%) slowed the curing process down slightly. Higher concentrations of the lamellar and needle-shaped pigment particles as well as of the lamellar core-shell pigments (at PVC=15%), on the contrary, brought about some drying rate decrease because oxygen penetrated more slowly through the film of this paint (drying by the oxypolymerization mechanism) [50]. The paint did not attain as high hardness levels during the measurement as the paints containing the isometric and smaller pigment particles.

Corrosion tests of the pigmented paints

The results of the corrosion tests of the paints containing the pigments studied are listed in Tables 4-5.

Results of corrosion tests in condensed moisture atmosphere at 40°C

The paint films on metallic substrates were exposed to the atmosphere with condensed moisture during 1008 hours. Nearly all films exhibited small blisters over their surface **Tab. 4**. Best resistant to the formation of the osmotic blisters was the paint with pigment *C* (lamellar $Mg_{0.2}Zn_{0.8}Fe_2O_4$) at PVC = 5%, where no blisters at all were observed on the film surface or near the test cut. At that PVC, the lamellar particles assumed a regular orientation during the paint film drying process, thereby enhancing the barrier effect. The resistance of this paint against blistering decreased if the pigment concentration was increased above the PVC = 5% level: at PVC =10%, blisters were observed and their occurrence was categorized as 6M (Fig. 2).

A high resistance against blistering was also observed with the paint containing pigment *Pig B* (acicular $Mg_{0.2}Zn_{0.8}Fe_2O_4$) at PVC = 5%: no blisters were observed on the film surface, and very few very small blisters was found near the test cut. Those blisters

were categorized as 8F (isolated occurrence of smallest blisters). Again, this paint film resistance was reduced (8M – 8D) as the PVC value was increased. The paint films containing the core-shell pigment *Pig D* (mixed *Mg–Zn–Fe oxide/kaolin*) also exhibited a good resistance to blistering. Slight blistering was observed both on the film surface and near the test cut at PVC = 10% and at PVC = 5% (category 8F). The paint with the isometric pigment *A* (isometric $Mg_{0.2}Zn_{0.8}Fe_2O_4$) was comparable, but only at PVC = 15%, where the occurrence of blisters on the film surface and near the cut was categorized as 8F.

The low resistance against the osmotic blister formation was observed for the paint containing the reference pigment *Pig F* (hematite Fe_2O_3) at PVC = 10%: the film was speckled with blisters over the whole surface (category 8D), and larger osmotic blisters were visible near the test cut (category 2M). Photographs of the films are shown in Figure 2, wherefrom a comparison of the resistance against blistering between the paints can be clearly made. Unlike the pigments synthesized, this pigment *F* does not provide adequate physical protection to the alkyd film or resistance against water vapour diffusion.

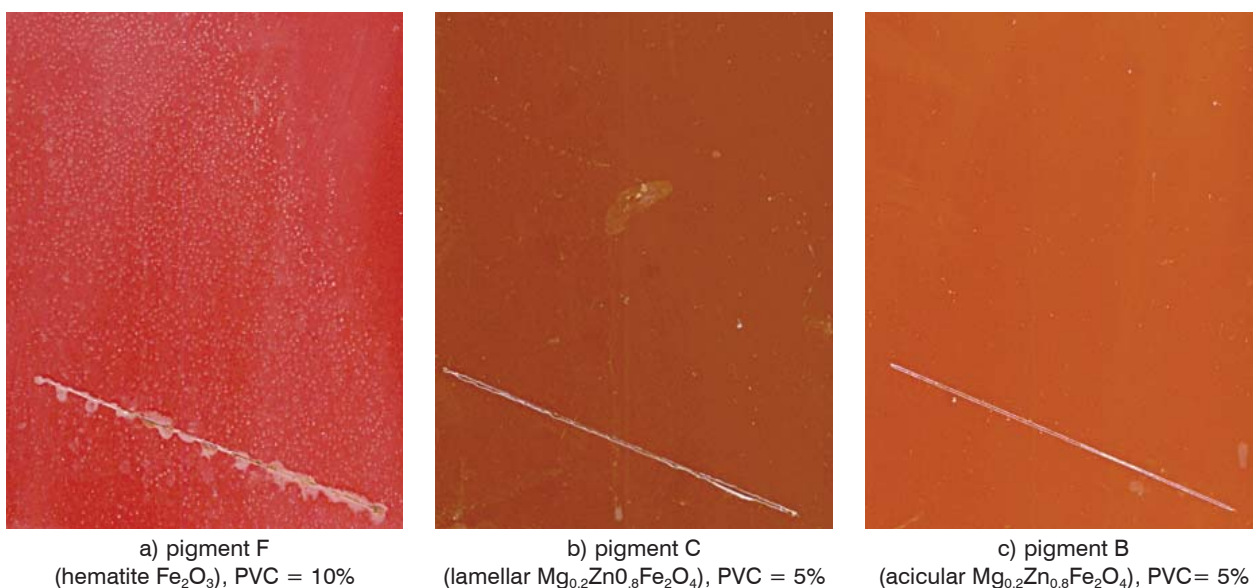


Fig. 2. Photographs of the coated steel panels
Obr. 2. Snímky ocelových panelů s nátěry

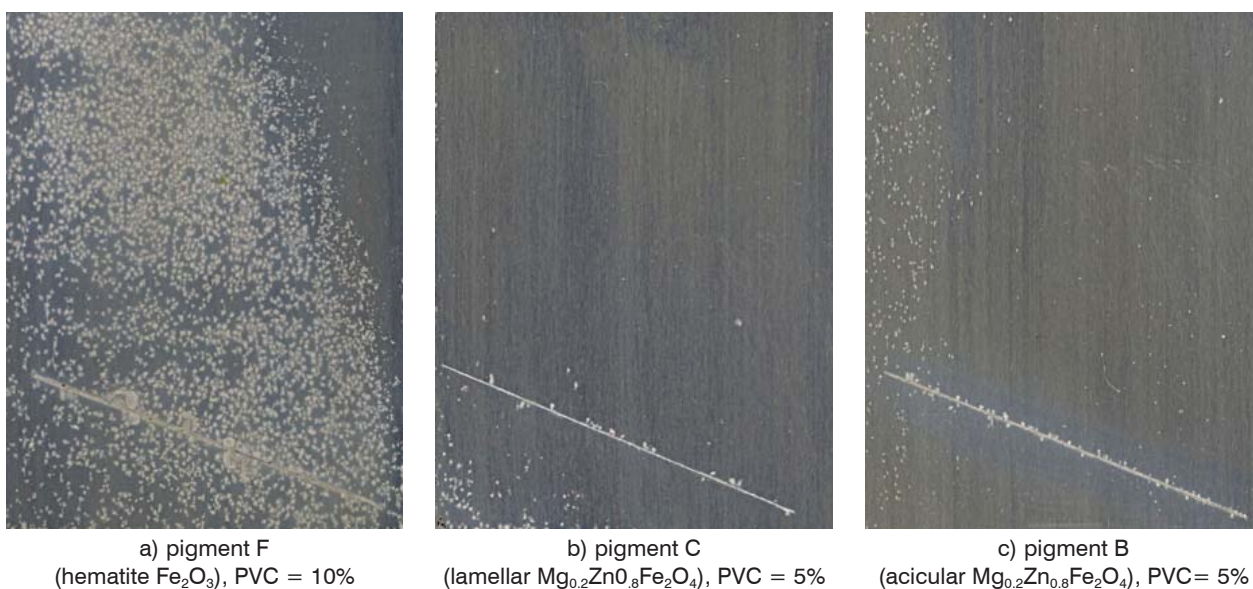


Fig. 3. Photographs of the steel panels after removing the paint films
Obr. 3. Snímky ocelových podkladů po odstranění nátěrů

The paint films were then removed from the steel panels and the panels were examined for corrosion on the metal surface and near the test cut. All the films were found to provide very good corrosion protection in the test cut (values of 0.5-1.0 mm). The best efficiency and best protection in the cut (0.0-0.5 mm) were observed for the paint with pigment C (lamellar $Mg_{0.2}Zn_{0.8}Fe_2O_4$) at PVC = 5%. Excellent results (0.0-0.05mm) were also obtained with the paint containing pigment A (isometric $Mg_{0.2}Zn_{0.8}Fe_2O_4$) at PVC = 10% and PVC = 15%.

Corrosion on the steel surface beneath the paint film was appreciable and differed significantly between the paints. Very good results were obtained with the paint with pigment A (isometric $Mg_{0.2}Zn_{0.8}Fe_2O_4$) at PVC = 15%, where the corroded surface area fraction was 0.1%. The best protection was provided by the paint containing pigment C (lamellar $Mg_{0.2}Zn_{0.8}Fe_2O_4$) at PVC = 5%: the steel surface was virtually free (0.03%) from corrosion. The protective ability, however, decreased appreciably if the PVC was increased, so that ultimately the corrosion reached 33% of the surface area. Hence, the optimum concentration of this pigment with respect to substrate protection against corrosion is PVC = 5%.

A similar degree of protection against corrosion on the steel panel surface was obtained with the paint containing pigment B (acicular $Mg_{0.2}Zn_{0.8}Fe_2O_4$) at PVC = 5% (corroded surface fraction 0.1%). This protective effect was lower if the pigment concentration was increased: the corroded surface fraction was 10% and 33% at PVC = 10% and at PVC = 15%, respectively.

Satisfactory substrate protection against corrosion was also achieved with the paint containing the core-shell pigment D (mixed Mg–Zn–Fe oxide/kaolin) up to PVC = 10% (3% surface area corroded), whereas the lowest protection was obtained with the paint containing the core-shell pigment E (mixed Mg–Zn–Fe oxide/talc). Here the corrosion on the steel surface decreased with increased pigment concentration: the corroded surface fraction was 50%, 33%, and 10% at PVC = 5%, PVC = 10%, and PVC = 15%, respectively.

The substrate surface corrosion was extensive (50% fraction affected) if the paint containing pigment F (hematite Fe_2O_3) at PVC = 10% was used. Photographs of the steel panels are shown in Figure 3, providing an illustrative comparison.

Tab. 4. Corrosion resistance of the paints (measured after 1008-hours' exposure of the steel panels in a steam chamber at an elevated temperature, DFT = $90 \pm 10 \mu\text{m}$) / Korozní odolnost nátěrů (měřeno po 1008 hodinové expozici nátěrů v komoře s obsahem vodní páry při zvýšené teplotě, DFT = $90 \pm 10 \mu\text{m}$)

Pigment	PVC (%)	Paint film		Steel panel		Anticorrosive efficiency E_{H2O}
		Degree of blistering		Corrosion in the cut (mm)	Metal surface corrosion (%)	
		Around the cut	On the film surface			
Pig A $Mg_{0.2}Zn_{0.8}Fe_2O_4$ isometric	5	4MD	8M	0.5 – 1.0	33	49
	10	6MD	8F	0 – 0.5	0.3	71
	15	8F	8F	0 – 0.5	0.1	84
Pig B $Mg_{0.2}Zn_{0.8}Fe_2O_4$ acicular	5	8F	–	0 – 0.5	0.1	90
	10	4MD	8M	0 – 1.0	10	54
	15	2MD	8D	0.5 – 1.0	33	44
Pig C $Mg_{0.2}Zn_{0.8}Fe_2O_4$ lamellar	5	–	–	0 – 0.5	0.03	98
	10	4M	6M	0.5 – 1.0	10	58
	15	–	6MD	0.5 – 1.0	33	44
Pig D Mg–Zn–Fe mixed oxide/kaolin	5	2M	8F	0.5 – 1.0	3	66
	10	4F	8F	0.5 – 1.0	3	73
	15	4F	6M	0 – 0.5	16	61
Pig E Mg–Zn–Fe mixed oxide/talc	5	4F	8D	0.5 – 1.0	50	40
	10	2M	8MD	0.5 – 1.0	33	44
	15	4M	6M	0.5 – 1.0	10	57
Pig F hematite Fe_2O_3	5	2M	8MD	0.5 – 1.0	33	45
	10	2MD	8D	0.5 – 1.0	50	29
	15	2MD	8F	0.5 – 1.0	10	64
Non pig. paint film	–	2D	8M	0.5 – 1.0	10	54

Most efficient with respect to corrosion protection in the atmosphere with condensed moisture were non-isometric pigments with lamellar or needle-shaped particles. The paints containing them were perfectly resistant to blistering and protected the substrate against corrosion very well [33]. Their concentration in the paint, however, is an important variable: in fact, their protective efficiency decreases sharply after the exceeding the optimum PVC level [43].

The following conclusions can be drawn from the findings:

- The highest anticorrosive protection was obtained with the nonisometric pigments **B** (*acicular* $Mg_{0.2}Zn_{0.8}Fe_2O_4$) and **C** (*lamellar* $Mg_{0.2}Zn_{0.8}Fe_2O_4$). Their optimum concentration in the binder was PVC = 5%. The efficiency of the isometric pigment **A** (*isometric* $Mg_{0.2}Zn_{0.8}Fe_2O_4$) increased with increasing PVC.
- If present at higher concentrations, isometric particles enhance the substrate metal protection against corrosion. In order to exhibit their barrier effect, the isometric particles must be present at higher concentration (PVCs), in contrast to lamellar particles, where the barrier effect is achieved at lower concentrations, specifically at PVC=5% in our case. The arrangement of the lamellar particles in the film plays an important role.
- The kaolin core of the appropriate core-shell pigment has a favourable effect on the paint's protective properties (at PVC = 5% or 10%). Talc is inferior to kaolin in this respect: the paint with the talc core protects the substrate surface to a lesser extent and blisters are observed near the cut.
- The core-shell pigments are inferior to the non-core-shell pigments as regards their efficiency in the atmosphere with condensed moisture at 40°C.
- Pigments that were efficient in slowing down corrosion in the high-humidity atmosphere had a lower fraction of water-soluble substances and contained smaller nonisometric particles (needle-shaped, lamellar). The pH of such pigments affects the efficiency of the paint to the extent that PVC = 5 is sufficient to inhibit the corrosion reactions. The use of the pigments at higher concentrations, however, is not that convenient.

The total anticorrosive efficiency was calculated for all the paints tested. Most efficient by that parameter was the protective film containing pigment **C** (*lamellar* $Mg_{0.2}Zn_{0.8}Fe_2O_4$) at PVC = 5% ($E_{H_2O} = 98$), followed by pigment **B** (*acicular* $Mg_{0.2}Zn_{0.8}Fe_2O_4$) also at PVC = 5% ($E_{H_2O} = 90$). The two pigments were able to strengthen the paint film in the constant humidity environment and so to increase its resistance to the formation of osmotic blisters and its protective capacity against metallic substrate corrosion.

Results of cyclic corrosion tests in the neutral salt mist atmosphere

No blisters on the paint film were found following the accelerated corrosion test in a neutral salt mist atmosphere. Since the values were identical for all the pigments, they are not included in Table 5. The anticorrosive efficiency in that atmosphere (E_{NaCl}) was therefore assessed based on the following effects: degree of paint film blistering near a test cut according to ASTM D 714-87; propagation (in mm) of the metal substrate corrosion in the cut according to ASTM D 1654-92; and degree of corrosion (%) on the metallic substrate surface according to ASTM D 610-85. Table 5 lists the results of corrosion resistance measurements in an atmosphere with a NaCl mist. The coated panels were exposed during 840 hours. Osmotic blisters were never observed on the paint film surface. The resistance to blister formation near the test cut, however, was different for the different paints. The paint films with pigment **A** (*isometric* $Mg_{0.2}Zn_{0.8}$) failed completely in this respect (score 2D). The paint film was wrinkled appreciably near the cut – the more the higher the PVC. This wrinkling effect was also observed with the paint containing pigment **B** (*acicular* $Mg_{0.2}Zn_{0.8}Fe_2O_4$), its extent, however, diminished with increasing PVC, to vanish completely at PVC = 15%, at which only a few small blisters were found around the test cut (score 4F). The paint that contained the pigment with needle-shaped particles was reinforced by the pigment at a sufficiently high PVC and blisters were formed to a lesser extent. This confirms the barrier and reinforcing properties of this pigment if present in an adequately high concentration [29,52].

The highest resistance against blistering around the cut was provided by the paint with pigment **C** (*lamellar* $Mg_{0.2}Zn_{0.8}Fe_2O_4$). In contrast to the needle-shaped pigment **B**, pigment **C** exerted this protective effect also at a low PVC. Outstanding resistance was found across the entire PVC range, particularly at PVC = 5% and at PVC = 10% (score 4F). Very good results (also score 4F) were obtained when using the paint containing the core-shell pigment **E** (*mixed* $Mg-Zn-Fe$ oxide/talc) at PVC = 10%. A similar resistance to blistering (score 2F) was exhibited by the paint with the core-shell pigment **D** (*mixed* $Mg-Zn-Fe$ oxide/kaolin) at PVC = 15%: the largest blisters were present around the cut at the lowest frequency of occurrence. However, this resistance to blistering dropped sharply with decreasing pigment concentration, and wrinkling around the cut (score 2D) appeared at PVC = 10%. These results illustrate well the situation where the isometric particles of pigment **A** (*isometric* $Mg_{0.2}Zn_{0.8}Fe_2O_4$) were unable to efficiently prevent formation of small osmotic blisters near the cut (score 2D). The paints with the nonisometric pigment **C** (*lamellar* $Mg_{0.2}Zn_{0.8}Fe_2O_4$) and with the core-shell pigment **D** (*mixed* $Mg-Zn-Fe$ oxide/kaolin) formed a good-quality protective barrier, and blistering near the cut was nearly invisible (score 4F at PVC=10%).

The paint films were removed from the steel panels in order to examine corrosion on the metal surface (beneath the initially present films) and corrosion propagation from the test cut. Corrosion around the cut, which copied the paint wrinkling, was higher (0.0-1.0 mm) if the paint contained pigment A (isometric $Mg_{0.2}Zn_{0.8}Fe_2O_4$). Similar effects were observed for the paints with low concentrations of pigment B (acicular $Mg_{0.2}Zn_{0.8}Fe_2O_4$). The corrosion in the cut was not very different between the majority of the paints and was fairly low (0.0 – 0.5 mm). The nonpigmented coating material was an exception where corrosion reached 2 mm. Nearly all of the pigmented paint films efficiently protected the metal against corrosion. The highest efficiency, i.e. no steel panel surface corrosion, was observed with the paint containing pigment C (lamellar $Mg_{0.2}Zn_{0.8}Fe_2O_4$). The paint with the core-shell pigment E (mixed Mg–Zn–Fe oxide/talc) was also very efficient: the corrosion effects were very small (0.03%). The lowest steel panel protection against corrosion was obtained with the paint containing the core-shell pigment D (mixed Mg–Zn–Fe oxide/kaolin), and moreover, the protective efficiency was the poorer the higher the PVC level (affected fraction 0.3% – 1% – 3% at PVC = 5%, 10%, and 15%, respectively). The results (Tab. 5) demonstrate the good substrate protection provided by the paint with pigment

C (lamellar $Mg_{0.2}Zn_{0.8}Fe_2O_4$), failure occurring with the paint containing pigment A (isometric $Mg_{0.2}Zn_{0.8}Fe_2O_4$), where appreciable corrosion is due to the paint film wrinkling near the test cut (2D). Owing to the barrier effect exerted by them, the lamellar particles of the core-shell pigments were able to adequately protect the substrate from the penetration of the chloride ions.

The highest anticorrosive efficiency was observed with the paint containing pigment C (lamellar $Mg_{0.2}Zn_{0.8}Fe_2O_4$). This paint exhibited a very good resistance to blistering owing to the barrier effect, and efficiently protected the substrate against corrosion due to the active component. Very good results were also obtained with the paint containing the core-shell pigment E (mixed Mg–Zn–Fe oxide/talc) at PVC = 10%.

The following conclusion can be drawn from the observations in this corrosive environment:

- Paints with pigments consisting of isometric particles did not provide adequate protection against paint blistering.
- Owing to their arrangement, lamellar particles formed an efficient physical barrier in the paint film.
- Pigments with needle-shaped particles were efficient to prevent paint film blistering only if present at the highest concentration tested, i.e. PVC = 15%.

Tab. 5. Corrosion resistance of the paints (measured after 840-hours' exposure in a NaCl atmosphere DFT = $90 \pm 10 \mu\text{m}$) / Korozní odolnost nátěrů (měřeno po 840 hodinové expozici nátěrů v atmosféře s obsahem s NaCl, DFT = $90 \pm 10 \mu\text{m}$)

Pigment	PVC (%)	Paint film	Steel panel		Anticorrosive efficiency E_{NaCl}
		Degree of blistering around the cut	Corrosion in the cut (mm)	Metal surface corrosion (%)	
Pig A $Mg_{0.2}Zn_{0.8}Fe_2O_4$ isometric	5	2D	0.5 – 1.0	0.1	58
	10	2D	0.5 – 1.0	0.1	58
	15	2D	0.5 – 1.0	0.1	58
Pig B $Mg_{0.2}Zn_{0.8}Fe_2O_4$ acicular	5	2D	0.5 – 1.0	0.1	58
	10	2D	0.5 – 1.0	0.03	60
	15	4F	0 – 0.5	3	75
Pig C $Mg_{0.2}Zn_{0.8}Fe_2O_4$ lamellar	5	4F	0 – 0.5	–	85
	10	4F	0 – 0.5	–	85
	15	2F	0 – 0.5	–	83
Pig D Mg–Zn–Fe mixed oxide/kaolin	5	2MD	0 – 0.5	0.3	67
	10	2D	0 – 0.5	1	57
	15	2F	0 – 0.5	3	73
Pig E Mg–Zn–Fe mixed oxide/talc	5	2MD	0 – 0.5	0.1	68
	10	4F	0 – 0.5	0.03	85
	15	2M	0 – 0.5	0.03	83
Pig F hematite Fe_2O_3	5	2MD	0 – 0.5	0.1	68
	10	2M	0 – 0.5	0.03	77
	15	4M	0 – 0.5	0.03	78
Non pigmented paint film	–	4MD	2.0 – 3.0	1	58

- Outstanding corrosion protection is provided by pigments with lamellar particles and core-shell pigments through the barrier effect of the core and through the active component in the mixed oxide form.

The above reasoning is supported by the calculated overall anticorrosive efficiency values, listed in Table 5. The highest overall anticorrosive efficiency was attained by using the paint with pigment *C* (lamellar $Mg_{0.2}Zn_{0.8}Fe_2O_4$) at PVC = 5% and 10% ($E_{NaCl} = 85$). The same result was obtained by using the paint with the core-shell pigment *E* (mixed *Mg–Zn–Fe oxide/talc*), whereas the lowest resistance was obtained for the paint with pigment *A* (isometric $Mg_{0.2}Zn_{0.8}Fe_2O_4$) ($E_{NaCl} = 58$). The anticorrosive efficiency is also insufficient if using pigment *B* (acicular $Mg_{0.2}Zn_{0.8}Fe_2O_4$) at low concentrations: the PVC must be $\geq 15\%$ to eliminate any blistering. Hence, the pigment with markedly lamellar particles was confirmed to be the best with respect to the protection against salt mist because this pigment made up a barrier against chloride ion penetration. It has been found [39] that efficient against corrosion in the salt mist environment are those pigments that act by the barrier effect exerted by the lamellar particles or by the core-shell particles [10]. As an additional advantage, the extract of the pigment with lamellar particles is alkaline and is able to neutralize the acidic corrosion products emerging during the action of the chloride ions on the steel panel in the moist atmosphere.

CONCLUSIONS

Anticorrosive efficiency was investigated for paint films containing one of three ferrosin ($Mg_{0.2}Zn_{0.8}Fe_2O_4$) based pigments or one of two core-shell-pigments consisting of Fe-Mg-Zn ferrite ($Mg_{0.2}Zn_{0.8}Fe_2O_4$) shell and lamellar silicate based cores. Every property of a pigmented paint is at its optimum at a specific pigment concentration; this applies particularly to the physical and anticorrosive properties [2,14,33]. So it is possible to identify a pigment concentration at which a specific property is at its best or at which the overall anticorrosive efficiency is at its maximum [37].

The ferrosin fall in the class of chemically acting pigments that help slow down corrosion processes on the metal surface beneath the paint film through their alkaline nature and by neutralization of the carboxy groups [48]. The lamellar shape of the pigment particles enhances paint film adhesion to the substrate and its cohesion and reduces the formation of blisters on the paint film surface (and around the test cut). None of the pigments had a substantial effect on the resin curing patterns, except for pigment *A* (isometric $Mg_{0.2}Zn_{0.8}Fe_2O_4$) which improved the paint film hardness.

In the accelerated corrosion tests in a condensed moisture atmosphere, the nonisometric pigments at PVC = 5% proved to be considerably more efficient as anticorrosive ingredients than the isometric pigments. In fact, the isometric pigment *A* (isometric $Mg_{0.2}Zn_{0.8}Fe_2O_4$) was efficient at PVC = 15% only. Pigments *C* (lamellar $Mg_{0.2}Zn_{0.8}Fe_2O_4$) and *B* (acicular $Mg_{0.2}Zn_{0.8}Fe_2O_4$) at PVC = 5% provided clearly the highest anticorrosive protection in the environment studied. They may find application in paints intended for increased humidity environments, in primers for bridge structures and in paints for the power sector. In the corrosion test in the neutral salt mist atmosphere, the ability of the nonisometric pigment *C* (lamellar $Mg_{0.2}Zn_{0.8}Fe_2O_4$) to exert a barrier effect dominated and the paint films with this pigment exhibited clearly the highest anticorrosive efficiency. This lamellar pigment may certainly find application in primers for structures in high-salt environments, such as street and road posts and steel structures in seaside areas.

It follows from the results that the morphology the pigment particles plays a major role in the paints' anticorrosive properties. Paints with nonisometric pigments gave better results than paints with isometric pigments during nearly all measurements. This is primarily due to the barrier effect to substances penetrating through the protective film. The best combined anticorrosive effect was found for pigment *C* with lamellar particles (lamellar $Mg_{0.2}Zn_{0.8}Fe_2O_4$). This pigment acted very favourably by the chemical inhibition mechanism; induced saponification in the alkyd resin owing to by its high alkalinity; and acted by the barrier effect. The core-shell pigments *D* (mixed *Mg–Zn–Fe oxide/kaolin*) and *E* (mixed *Mg–Zn–Fe oxide/talc*), which also exhibit very good anticorrosive efficiency in many parameters, may also be used as convenient variants: they are less expensive than pigment *C* and contain less zinc because the mineral core represents a considerable fraction of the pigment particle weight. Core-shell pigments represent an economical solution for the synthesis of anticorrosive pigments [27,28] obtained by the high-temperature reaction. Moreover, talc and kaolin are natural materials which are reasonably well available and are environmentally and toxicologically acceptable.

REFERENCES

1. Kalendova A. et al. Anticorrosion efficiency of zinc-filled epoxy coatings containing conducting polymers and pigments, *Progress in Organic Coatings* **2015**, 78, 1-20.
2. Benda P., Kalendova A. Anticorrosion properties of pigments based on ferrite coated zinc particle, *Physica Procedia* **2013**, 44, 185-194.
3. Kos I., Schwarz I. G., Suton K. Influence of Warp Density on Physical-mechanical Properties of Coated Fabric, *Procedia Engineering* **2014**, 69, 881-889.

4. Kohl M., Kalendova A. Effect of polyaniline salts on the mechanical and corrosion properties of organic protective coatings, *Progress in Organic Coatings* **2015**, 86, 96-107.
5. Anez L. et al. Gas and liquid permeability in nano composites get: Comparison of Knudsen and Klinkenberg correction factors, *Microporous and Mesoporous Materials* **2014**, 200, 79-85.
6. Marzi T. Nanostructured materials for protection and reinforcement of timber structures: A review and future challenges, *Construction and Building Materials* **2015**, 97, 119-130.
7. Šadauskienė J. et al.: The impact of the exterior painted thin-layer render's water vapour and liquid water permeability on the moisture state of the wall insulating system, *Construction and Building Materials* **2009**, 23 (8), 2788-2794.
8. Ulbrich M., Kalendova A. Properties of Organic Coatings with Nonisometric Ferrite particles, *Physics Procedia* **2013**, 44, 247-255.
9. Du J. et al. Simulation of the neck growth of non-isometric biosphere during initial sintering, *Acta Metallurgica Sinica (English letters)* **2009**, 22 (4), 263-274.
10. Singh S. et al. Magnetodielectric effect in BaTiO₃/ZnFe₂O₄ core/shell nanoparticles, *Journal of Alloys and Compounds* **2014**, 587, 437-441.
11. Liu C. et al. Structural analysis and characterization of doped spinel CO_{2-x}M_xTiO₄ (M = Mg²⁺, Mn²⁺, Cu²⁺ and Zn²⁺) coated mica composite. *Ceramions International* **2015**, 41, 5537-5546.
12. Naredi R., Mahdavian M., Darvish A. Electrochemical examining behavior of epoxy coating incorporation zinc-free phosphate-based anticorrosion pigment, *Progress in Organic Coatings* **2016**, 76, 302-306.
13. Darvish A., Naredi R., Attar M.M. The impact of pigment volume concentration on the protective performance of polyurethane coating with second generation of phosphate based anticorrosion pigment, *Progress in Organic Coatings* **2014**, 77, 1768-1773.
14. Sadek M.E.H. et al. Nano Mg_{1-x}Ni_xAl₂O₄ spinel pigments for advanced applications, *Spectrochimica Acta Part A: Molecular and Biomolecular Spectroscopy* **2014**, 125, 353-358.
15. Li J. et al. In-situ AFM and EIS study of a solventborne alkyd coating with nanoclay for corrosion protection of carbon steel, *Progress in Organic Coatings* **2015**, 87, 179-188.
16. Gergely A et al.. Corrosion protection with zinc-rich epoxy paint coatings embedded with various amounts of highly dispersed polypyrrole-deposited alumina monohydrate, *Progress in Organic Coatings* **2013**, 76, 17-32.
17. Sickafus K.E., Wills J.M., Grimes N.W. Structure of spinel, *Journal of the American Ceramic Society* **1999**, 82 (12), 3279-3292.
18. Giannakas A.E. et al. Surface properties, textural features and catalytic performance for NO + CO abatement of spinels MA₂O₄ (M = Mg, Co and Zn) developed by reverse and bicontinuous microemulsion method, *Applied Surface Science* **2007**, 253 (16), 6969-6979.
19. Huang C.L. et al. Low-loss microwave dielectrics in spinel-structured (Mg_{1-x}Ni_x)Al₂O₄ solid solutions, *Journal of the American Ceramic Society* **2010**, 93 (7), 1999-2003.
20. Jacob K.T., Alcock C.B. Activities and their relation to cation distribution in NiAl₂O₄ MgAl₂O₄ spinel solid solutions, *Journal of Solid State Chemistry* **1977**, 20 (1), 79-88.
21. Singh Yadav R. Impact of Nd³⁺ in CoFe₂O₄ spinel ferrite nanoparticles on cation distribution, structural and magnetic properties, *Journal of Magnetism and Magnetic Materials* **2016**, 339, 109-117.
22. Abdur Rehman M., Yusoff I., Alias Y. Fluoride adsorption by doped and un-doped magnetic ferrites CuCl_xFe_{2-x}O₄: Preparation, characterization, optimization and modeling for effectual remediation technologies, *Journal of Hazardous Materials* **2015**, 299, 316-324.
23. Porta P., Stone F.S., Turner R.G. The distribution of nickel ions among octahedral and tetrahedral sites in NiAl₂O₄, MgAl₂O₄ solid solutions, *Journal of Solid state Chemistry* **1974**, 11 (2), 135-147.
24. Sun K. Cation distribution and magnetic property of Ti/Sn - substituted manganese-zinc ferrites, *Journal of Alloys and Compounds* **2015**, 650, 363-369.
25. Fernandez A.L., de Pablo L. Formation and the colour development in cobalt spinel pigments. *Pigment & Resin Technology* **2002**, 31 (6), 350-356.
26. Zawrah M.F., Mاماad H., Meky S. Synthesis and characterization of nano MgAl₂O₄ spinel by the co-precipitated method, *Ceramic International* **2007**, 33 (6), 969-978.
27. Neto J.B.R., Moreno R. Rheological behaviour of kaolin/talc/alumina suspensions for manufacturing cordierite foams, *Applied Clay Science* **2007**, 37 (1-2), 157-166.
28. Li Z. et al. Fabric effect on hydraulic conductivity of kaolin under different chemical and biochemical conditions, *Soils and Foundations* **2013**, 53 (5), 680-691.
29. Veselý D., Kalendová A. Anticorrosion efficiency of Zn_xMg_yAl₂O₄ core-shell spinels in organic coatings, *Progress in Organic Coatings* **2008**, 62, 5-20.
30. Jotti K.J., Palanivelu K. Facile fabrication of core-shell Pr₆O₁₁-ZnO modified silane coatings for anti-corrosion applications, *Applied Surface Science* **2014**, 288, 60-68.
31. Kalendova A., Vesely D. Study of the anticorrosive efficiency of zincite and periclase-based core-shell pigments in organic coatings, *Progress in Organic Coatings* **2009**, 64 (1), 5-19.
32. Montemor M.F. Functional and smart coatings for corrosion protection: A review of recent advances, *Surface and Coatings Technology* **2014**, 258, 17-37.
33. Kalendova A., Rysanek P., Nechvilova K. Investigation of the anticorrosive efficiency of ferrites Mg_{1-x}Zn_xFe₂O₄ with different particle morphology and chemical composition in epoxy-ester resin-based coatings, *Progress in Organic Coatings* **2015**, 86, 147-163.
34. Vesely D., Kalendova A., Manso M. V. Properties of calcined kaolins in anticorrosion paints depending on PVC, chemical composition and shape of particles, *Progress in Organic Coatings* **2012**, 74, 82-91.
35. Kalendova A. Effect of surface treatment of pigment particles with polypyrrole and polyaniline phosphate on their corrosion inhibiting properties in organic coatings, *Progress in Organic Coatings* **2014**, 77 (9), 1465-1483.
36. Singh A.P. et al. Fatty acid based waterborne air drying epoxy ester resin for coating applications, *Progress in Organic Coatings* **2015**, 87, 95-105.
37. Gao X.Z., Liu H.J., Cheng F. Thermoresponsive polyaniline nanoparticles: Preparation, characterization, and their potential application in waterborne anticorrosion coating, *Chemical Engineering Journal* **2016**, 283, 682-691.

38. Kalendova A. Methods for testing and evaluating the flash corrosion. *Progress in Organic Coatings* **2002**, 44 (3), 201-209.
39. Conradi M. et al. Mechanical and anticorrosion properties of nanosilica-filled epoxy-resin composite coating. *Applied Surface Science* **2014**, 292, 432-437.
40. Czech office for standards, metrology and testing. **2007** Czech technical standard: Coating compositions. Determination of hardness of painting film by pendulum instrument. CSN 67 3076. Praha.
41. Hao Y., Liu F., Man E. Inhibite Behaviour and Mechanism of a Ferrite Inhibition Pigment en Epoxy Paints, *Journal of the Electrochemical Society* **2012**, 159 (9), C403-C410.
42. Lin G. et al. Some nanocomposites based on a glycerol-derived alkyd resin and layered silicates, *Molecular Crystals and Liquid Crystals* **2008**, 483 (1), 33-48.
43. Naderi R., Attar M.M. Electrochemical study of protective behavior of organic coating pigmented with zinc aluminium phosphate as a modified zinc phosphate at different pigment volume concentrations, *Progress in Organic Coatings* **2009**, 66 (3), 314-320.
44. Perra D.Y. Effect of pigmentation on organic coating characteristics, *Progress in Organic Coatings* **2004**, 50 (4), 247-262.
45. Bierwagen G.P., Hay T.K. The reduced pigment volume concentration as an important parameter in interpreting and predicting the properties of organic coatings, *Progress in Organic Coatings* **1975**, 3 (4), 281-303.
46. Gowri S., Balakrishman K. The effect of the PVC/CPVC ratio on the corrosion resistance properties of organic coating, *Progress in Organic Coatings* **1994**, 23 (4), 363-377.
47. Langer E. et al. Self-stratifying coatings containing barrier and active anticorrosive pigments, *Progress in Organic Coatings* **2011**, 71, 162-166.
48. Ahmed N.M. et al. Novel anticorrosive pigments based on waste material for corrosion protection of reinforced concrete steel, *Construction and Building Materials* **2015**, 98, 399-396.
49. Deyab M.A. Effect of carbon nano-tubes on the corrosion resistance of alkyd coating immersed in sodium chloride solution, *Progress in Organic Coatings* **2015**, 85, 146-150.
50. Lamanna M.E. Synthesis of an organic semiconductor by polymerization of 3-amino-1,2,4-triazole, *Reactive and Functional Polymers* **2009**, 69 (10), 759-765.
51. Liu L. et al. The evaluation of thermal performance of cool coatings colored with high mera-infrared reflective nanobrown inorganic pigments: Magnesium doped ZnFe₂O₄ compounds, *Solar Energy* **2015**, 113, 48-56.
52. Emira H. S., Abdel-Mohsen F.F. The dependence of the corrosion protection of water-borne paints on the concentration of the anticorrosive pigment, *Pigment & Resin technology* **2003**, 32 259-263.